Spin Manipulation in Co-Doped ZnO

Qingyu Xu,[1,*] Lars Hartmann,[2] Shengqiang Zhou,[1] Arndt Mcklich,[1] Manfred Helm,[1] Gisela Biehne,[3] Holger Hochmuth,[3]
Michael Lorenz,[3] Marius Grundmann,[3] and Heidemarie Schmidt[1]

[1]*Institut für Ionenstrahlphysik und Materialforschung, Forschungszentrum Dresden-Rossendorf e.V.,*
Bautzner Landstraße 128, 01328 Dresden, Germany
[2]*Solarion AG/Photovoltaics, Ostende 5, 04288 Leipzig, Germany*
[3]*Universität Leipzig, Fakultät für Physik und Geowissenschaften, Institut für Experimentelle Physik II,*
Linnéstrasse 5, 04103 Leipzig, Germany
(Received 28 April 2008; published 11 August 2008)

We report the clearly observed tunneling magnetoresistance at 5 K in magnetic tunnel junctions with
Co-doped ZnO as a bottom ferromagnetic electrode and Co as a top ferromagnetic electrode prepared by
pulsed laser deposition. Spin-polarized electrons were injected from Co-doped ZnO to the crystallized
Al_2O_3 and tunnelled through the amorphous Al_2O_3 barrier. Our studies demonstrate the spin polarization
in Co-doped ZnO and its possible application in future ZnO-based spintronics devices.

Both charge and spin degrees of freedom play an important and indispensable role in realizing functionalities in future semiconductor spintronics [1]. The manipulation of spins in spintronics consists of three processes: spin generation, transport, and detection [2]. Nowadays, ferromagnetic metals are successfully used to generate polarized spins for the injection into semiconductors, but the efficiency of the spin injection from ferromagnetic metals to semiconductors is very low, due to the large mismatch of the resistance between metals and semiconductors [2,3]. Diluted magnetic semiconductors (DMSs) are considered to be very important materials in future semiconductor spintronics applications due to the simultaneous control of electrons' charge and spin. DMS materials combining semiconducting *and* magnetic properties are expected to improve the efficiency of spin injection. Mn-doped GaAs is a successful DMS which has been studied in the context of spintronics applications [4,5]. However, the Curie temperature below 173 K limits applications at room temperature [6]. For practical applications, a DMS exhibiting ferromagnetism at room temperature (or above) is required. ZnO has been studied extensively for different magnetic dopants after the theoretical prediction of room temperature ferromagnetism in magnetic doped ZnO [7–9]. The published experimental results on magnetic properties are contradictory [10], and, until now, the research work on ZnO is still concentrating on the realization of intrinsic ferromagnetism [11,12]. However, the demonstration of the spin polarization in Co-doped ZnO is still lacking.

Recently, Song *et al.* published a study on spin polarization in Co-doped ZnO-based magnetic tunnel junction (MTJ) structures [13,14]. However, the reported tunneling magnetoresistance (TMR) [13,14] is similar to the magnetoresistance (MR) probed on single layer Co-doped ZnO films [15]. On the other hand, Co-doped ZnO has been classified as being a ferromagnetic semiconductor by the theoretical work and magnetization measurements [7–9,12], which needs further demonstration by spin-polarized transport properties. Here we report on spin manipulation in Co-doped ZnO and the observation of TMR in a MTJ using Co-doped ZnO as one ferromagnetic electrode. The clear demonstration of the spin manipulation in Co-doped ZnO greatly facilitates the final application of magnetic doped ZnO in future semiconductor spintronics devices.

The Al-doped ZnO buffer layer, the Co-doped ZnO bottom electrode, and the Al_2O_3 barrier layer were subsequently deposited on *a*-plane sapphire substrates by pulsed laser deposition (PLD) from the ceramic targets $Zn_{0.99}Al_{0.01}O$, $Zn_{0.945}Co_{0.05}Al_{0.005}O$, and Al_2O_3, respectively. Circular Co dots with an area of 2.3×10^{-3} cm^2 (diameter 540 μm) were deposited by thermal evaporation in a BAL-TEC MED020. The thickness of each layer was controlled by the number of laser pulses with an energy density of 2 $J\,cm^{-2}$. The cross-sectional transmission electron microscopy (TEM) images were taken by an FEI Titan 80–300 S/TEM. The exact composition of Co-doped ZnO was determined to be $Zn_{0.91}Co_{0.09}O$ by combined Rutherford backscattering spectrometry (RBS) and particle-induced x-ray emission (PIXE) measurements. The thickness of Co-doped ZnO and Al-doped ZnO determined by TEM was 180 and 220 nm, respectively. The thickness of Al_2O_3 was selected when the resistance of the junction sample drastically increased with increasing Al_2O_3 layer thickness [16]. Magnetotransport measurements with the field applied in the film plane were performed in two-point geometry as shown in Figs. 1(a) and 1(b) at 5 K. A constant current was applied by a Keithley 2400 source meter for the MR measurements. The *M-H* loop was measured by a superconducting quantum interference device magnetometer with the magnetic field applied in the film plane at 5 K. The applied maximum magnetic field was 6 T.

Though doping with Al can greatly improve the conductivity of ZnO, the resistance is still too large after
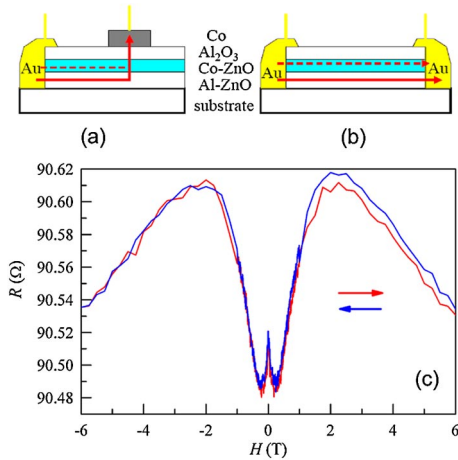
FIG. 1 (color online). Two-point measurements for (a) TMR structure and (b) bottom electrode on the MTJ sample. The red arrows indicate the moving direction of the electrons. (c) The MR effect at 5 K of the bottom electrode measured in (b); the arrows show the field sweep direction.

patterning Al-doped ZnO into several micrometer-wide stripes as the bottom electrode of the MTJ structure. Thus, an alternative geometry was applied for measuring the TMR effect, as shown in Fig. 1(a). The large area makes the resistance of the bottom electrode small, on the order of 100 Ω, which is much smaller than the junction resistance. Because of the double layer structure of the Al_2O_3 barrier layer (which will be explained later), the flowing direction of electrons is important for the final explanation of the observed spin-polarized transport phenomenon. During the measurements, the higher voltage was applied on the Co top electrode and lower voltage on the ZnO bottom electrode through the Au contact; thus, the current will pass from the Co top electrode to the ZnO bottom electrode. Since the charge carriers are electrons with negative charges, the electrons will pass from the ZnO bottom electrode to the Co top electrode, as the red arrows show in Fig. 1(a). The Ohmic contacts on doped ZnO were confirmed by the linear *I-V* curves measured by the two-point geometry shown in Fig. 1(b). The MR effects of the bottom electrode [Fig. 1(c)], namely, the Al-doped and Co-doped ZnO layers together, have been measured in the geometry shown in Fig. 1(b). The observed small negative MR at low field has been observed on single Al-doped ZnO layers [17]. The positive MR at intermediate field and negative MR at high field originate from Co-doped ZnO [15]. Because of the thickness-dependent defect formation of Co-doped ZnO, small inhomogeneities of Co-doped ZnO will strongly influence the current flow, with very thin Co-doped ZnO films being highly resistive [18]. However, the resistance is very small measured in the geometry of Fig. 1(b) with the current in plane for the parallel alignment of the highly conductive Al-doped ZnO and highly resistive Co-doped ZnO. As the positive MR is

very strong in highly resistive Co-doped ZnO [15], the positive MR can still be observed in the geometry of Fig. 1(b). Thus, we conclude that the current passes through the Al-doped ZnO layer and the Co-doped ZnO layer, as shown by the red lines in Figs. 1(a) and 1(b). In the MTJ structure shown in Fig. 1(a), the current tunnels with the highest probability perpendicular from the bottom electrode through the Al_2O_3 barrier layer to the Co top electrode.

Figure 2 shows the field dependence of resistance at 5 K with different applied constant currents. The MR curves contain two main parts: the butterfly MR curves below 1 T, which do not coincide, and the MR curves at fields above 1 T, which coincide for the field swept from 6 to −6 T and from −6 to 6 T. It must be noted that the MR curves at high field ($H > 1$ T) are very similar to the MR curves probed on single layer Co-doped ZnO [15], though the magnitude of resistance changes with different applied current. As explained already, the resistivity in Co-doped ZnO is not uniform, and a highly resistive Co-doped ZnO layer exists [18]. The resistance is very large measured in the geometry of Fig. 1(a) with the current perpendicular to the layer for the serial alignment of the highly conductive Al-doped ZnO and highly resistive Co-doped ZnO layers. We tend to relate the high field MR ($H > 1$ T) behavior of the investigated MTJ sample to the MR of the Co-doped ZnO [15].

The main, most interesting phenomenon is the low field butterfly positive MR behavior, as shown in Fig. 2. In contrast to the normally observed TMR effect, double peaks have been observed in each swept curve which locate at both sides of 0 T. We label the lower peak at the starting field minor peak and the higher peak at the end field major peak for each sweep direction. As one can see, with increasing applied current, the MR effect becomes weaker, which is a typical phenomenon of TMR [19]. When applying a current of 1 μA, the butterfly positive MR disap-
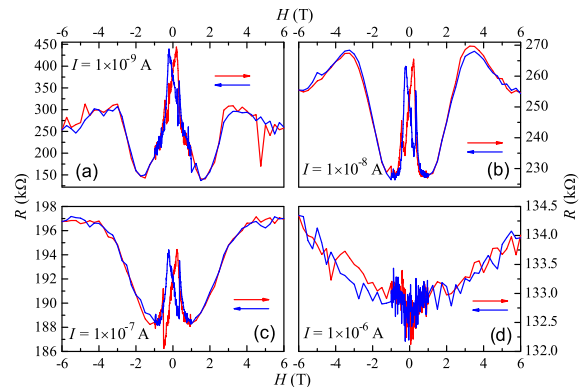

FIG. 2 (color online). Field-dependent resistance of the TMR sample measured at 5 K with field applied in the film plane in the geometry shown in Fig. 1(a). The applied constant current is (a) 1×10^{-9} A, (b) 1×10^{-8} A, (c) 1×10^{-7} A, and (d) 1×10^{-6} A. The arrows show the field sweep direction.

pears. The junction was destroyed, and no butterfly positive MR at low field could be observed afterwards even with a smaller applied current. Figure 3(a) shows the MR curve with 0.01 μA applied current before and after applying 1 μA. A clear butterfly positive MR can be seen in the curve before applying 1 μA [Fig. 2(d)]. After applying 1 μA [Fig. 2(d)], no such MR behavior can be observed anymore even with 0.01 μA. The disappearance of the butterfly positive MR behavior at low field is due to the broken junction after applying a large current; thus, the difference of the resistance before and after applying 1 μA can be roughly attributed to the tunnel resistance of the MTJ sample. Figure 3(b) shows the difference of resistance calculated from MR curves shown in Fig. 3(a). At 0 T, the junction resistance is on the order of 10 kΩ, which is 1 order smaller than the total resistance of the sample (on the order of 100 kΩ) but much larger than the resistance of the bottom electrode (on the order of 100 Ω). Figure 3(c)
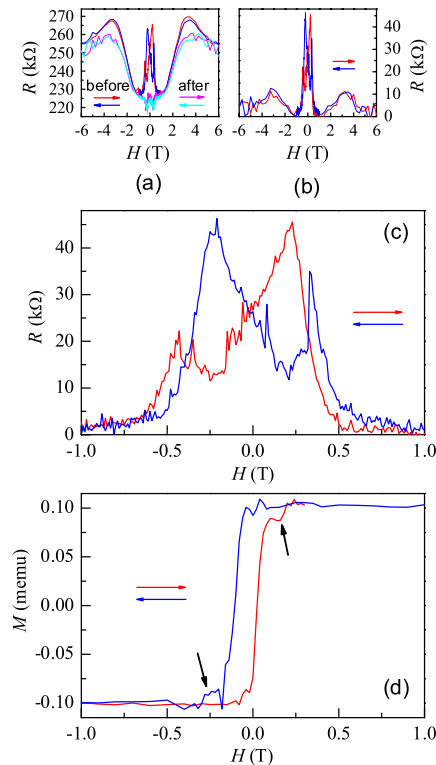

FIG. 3 (color online).   (a) The field dependence of resistance of the TMR sample measured at 5 K in the geometry shown in Fig. 1(a) applying a constant current of 1×10^{-8} A before and after the application of 1 μA [Fig. 2(d)] with field applied in the film plane. (b) The field-dependent resistance difference by subtracting the resistance before and after applying 1 μA is shown in (a). (c) The zoom view of the MR curve shown in (b) with field from -1 to 1 T. (d) The magnetization curve of the TMR sample at 5 K. The arrows indicate the field sweep direction. Besides the major loop with larger magnetization and smaller coercivity ($\sim$0.05 T), another loop with smaller magnetization and larger coercivity ($\sim$0.25 T) can also be seen, as shown by the short black arrows.

shows the MR curve in the range from -1 to 1 T, and Fig. 3(d) shows the field-dependent magnetization curve with the field applied in the film plane. Besides the narrow major loop with larger magnetization and smaller coercivity from the Co top electrodes, another loop as indicated by black arrows in Fig. 3(d) with small magnetization and larger coercivity due to the Co-doped ZnO bottom electrode can also be seen. However, normally the coercivity in ferromagnetic ZnO is small ($<$0.1 T) [20]. The larger coercivity ($\sim$0.25 T) in this Co-doped ZnO with an underlying Al-doped ZnO buffer layer might be related to the different strain and defect formation compared to Co-doped ZnO directly deposited on sapphire. The two-step reversal in the magnetization curve [Fig. 3(d)] indicates a good decoupling of the two magnetic layers, so that an antiparallel alignment of the magnetization is obtained between the two coercive fields. With increasing the field above the position of the major peak at $\sim$0.25 T, the resistance starts to decrease. This can be explained by the change from antiparallel to parallel aligned magnetization in the Co top electrode and in the Co-doped ZnO bottom electrode. The magnetic fields corresponding to the different transitions in the MR curves are larger than those observed for the magnetization curve. This is due to the fact that the tunneling is sensitive to the magnetization of the interface, which can switch at higher field than the bulk [21]. However, no indication is observed in M-H loop, which could be related to the observed minor peaks in MR curves. A similar MR curve was observed in the $SrTiO_3$/$LaAlO_3$ interface; the additional suppression around zero field might be due to additional spin or domain reorientation effects [22].

The cross-sectional TEM image of the MTJ sample is shown in Fig. 4(a). The thickness of the Al_2O_3 layer amounts to about 100 nm. After the growth of about 80 nm crystallized Al_2O_3, the structure changes to about 20 nm nearly amorphous Al_2O_3. A sharp interface can be clearly seen in the Al_2O_3 layer. The contrast in the 80 nm
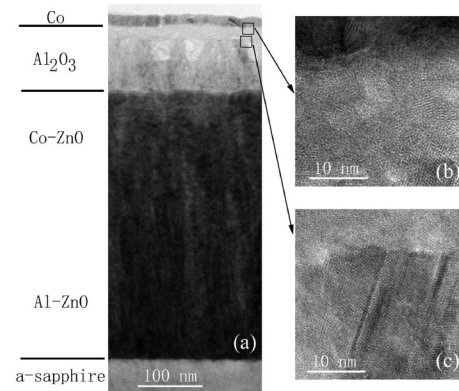

FIG. 4.   (a) The cross-sectional TEM image of the TMR sample. (b) and (c) are the HREM images taken from the marked region in (a).

crystallized Al_2O_3 layer is due to the different orientation of the grains. The change of the orientation of the grains during growth might relate to the final nearly amorphous Al_2O_3 layer. The elemental distribution profile measured by energy dispersive x ray (EDX) (with resolution of at least 0.5 at. %) in scanning transmission electron microscopy (STEM) mode confirms that these two layers are both Al_2O_3. The high resolution electron microscopy (HREM) images show that the bottom thicker Al_2O_3 layer is crystallized with columnar grain structure and the top thinner Al_2O_3 layer is almost amorphous. However, detailed investigation of the structure of the thinner amorphous Al_2O_3 layer indicates that this layer has small crystallized Al_2O_3 grains with random orientations. The approximately 80 nm thick crystallized Al_2O_3 layer is expected to be more conductive due to high defect density, while the approximately 20 nm thick amorphous Al_2O_3 layer will act as a tunneling barrier due to its nearly amorphous structure [16]. Though 20 nm is too thick for tunneling, the thickness of amorphous Al_2O_3 layer might not be uniform. Also, residual small grains may reduce the effective tunneling barrier thickness. The resistance of the junction is not very high, even 1 order smaller than the whole sample. With this Al_2O_3 layer structure in mind, we can understand the spin manipulation process in the MTJ structure. The spin-polarized current is generated in the Co-doped ZnO bottom electrode, and polarized spins will be injected into the thicker crystallized Al_2O_3 layer. Normally, the spin coherence length in semiconductors is extremely long [23]; the spin polarization will be conserved in the 80 nm thick crystallized Al_2O_3 layer. Then tunneling occurs at the 20 nm thick amorphous Al_2O_3 layer, and the polarized spins are detected by the Co top electrode. Thus, in the presented MTJ structure, spin generation in DMS (Co-doped ZnO), spin injection from DMS to crystalline Al_2O_3, and spin-polarized tunneling through amorphous Al_2O_3 have been realized.

In summary, MTJ samples with Co-doped ZnO as the bottom ferromagnetic electrode and Co as the top ferromagnetic electrode have been prepared by PLD. An Al_2O_3 barrier layer has been successfully prepared on Co-doped ZnO with a crystallized structure in the bottom and a nearly amorphous structure in the top. A clear TMR effect observed at 5 K demonstrates the spin-polarized transport including the spin injection from Co-doped ZnO to the crystallized Al_2O_3 and tunneling through the amorphous Al_2O_3. Our results demonstrate the spin polarization in Co-doped ZnO and its possible application in future spintronics devices with ZnO-based DMS.

*Corresponding author.
xuqingyu_1974@yahoo.com

[1] H. Akinaga and H. Ohno, IEEE Trans. Nanotechnol. **1**, 19 (2002).
[2] I. Žutić, J. Fabian, and S. Das Sarma, Rev. Mod. Phys. **76**, 323 (2004).
[3] G. Schmidt et al., Phys. Rev. B **62**, R4790 (2000).
[4] Y. Ohno et al., Nature (London) **402**, 790 (1999).
[5] M. Tanaka and Y. Higo, Phys. Rev. Lett. **87**, 026602 (2001).
[6] T. Jungwirth et al., Phys. Rev. B **72**, 165204 (2005), and references therein.
[7] T. Dietl et al., Science **287**, 1019 (2000).
[8] K. Sato and H. Katayama-Yoshida, Jpn. J. Appl. Phys. **39**, L555 (2000).
[9] K. Sato and H. Katayama-Yoshida, Jpn. J. Appl. Phys. **40**, L334 (2001).
[10] C. Liu, F. Yun, and H. Morkoç, J. Mater. Sci.: Mater. Electron. **16**, 555 (2005).
[11] M. Gacic et al., Phys. Rev. B **75**, 205206 (2007).
[12] A. J. Behan et al., Phys. Rev. Lett. **100**, 047206 (2008).
[13] C. Song et al., Appl. Phys. Lett. **91**, 042106 (2007).
[14] C. Song et al., Appl. Phys. Lett. **91**, 172109 (2007).
[15] Q. Xu et al., Phys. Rev. B **73**, 205342 (2006).
[16] We controlled the Al_2O_3 layer thickness by the laser pulse number. The resistance of the MTJ will increase abruptly with increasing the laser pulse number (thickness of the Al_2O_3 layer) above a critical value. The thickness of the Al_2O_3 layer of the sample studied in this Letter is just above this critical value. The TEM investigation shows that the bottom Al_2O_3 layer was polycrystalline, and the top part was nearly amorphous, indicating the structure change during the growth of the Al_2O_3 layer. The interdiffusion between neighboring layers has been excluded by EDX. Thus we can conclude that the crystallized Al_2O_3 layer is conductive. The drastic increase of resistance of the MTJ sample is due to the formation of the top amorphous Al_2O_3 layer. Spin-polarized electrons tunneled through this amorphous Al_2O_3 layer.
[17] T. Fukumura et al., Appl. Phys. Lett. **75**, 3366 (1999).
[18] Q. Xu et al., J. Appl. Phys. **100**, 013904 (2006).
[19] J. S. Moodera et al., Phys. Rev. Lett. **74**, 3273 (1995).
[20] S. A. Chambers et al., Mater. Today **9**, 28 (2006).
[21] J. M. De Teresa et al., Phys. Rev. Lett. **82**, 4288 (1999).
[22] A. Brinkman et al., Nature Mater. **6**, 493 (2007).
[23] J. H. Lee, S. Y. Park, Kyung-In Jun, K.-H. Shin, Jinki Hong, K. Rhie, and B. C. Lee, Phys. Status Solidi B **241**, 1506 (2004).